ACS APPLIED MATERIALS & INTERFACES

Research Article

www.acsami.org

α-Fe_2O_3@PANI Core–Shell Nanowire Arrays as Negative Electrodes for Asymmetric Supercapacitors

Xue-Feng Lu, Xiao-Yan Chen, Wen Zhou, Ye-Xiang Tong, and Gao-Ren Li*

MOE Laboratory of Bioinorganic and Synthetic Chemistry, KLGHEI of Environment and Energy Chemistry, School of Chemistry and Chemical Engineering, Sun Yat-sen University, Guangzhou 510275, China

Supporting Information

ABSTRACT: Highly ordered three-dimensional α-Fe_2O_3@PANI core–shell nanowire arrays with enhanced specific areal capacity and rate performance are fabricated by a simple and cost-effective electrodeposition method. The α-Fe_2O_3@PANI core–shell nanowire arrays provide a large reaction surface area, fast ion and electron transfer, and good structure stability, which all are beneficial for improving the electrochemical performance. Here, high-performance asymmetric supercapacitors (ASCs) are designed using α-Fe_2O_3@PANI core–shell nanowire arrays as anode and PANI nanorods grown on carbon cloth as cathode, and they display a high volumetric capacitance of 2.02 mF/cm^3 based on the volume of device, a high energy density of 0.35 mWh/cm^3 at a power density of 120.51 mW/cm^3, and very good cycling stability with capacitance retention of 95.77% after 10 000 cycles. These findings will promote the application of α-Fe_2O_3@PANI core–shell nanowire arrays as advanced negative electrodes for ASCs.

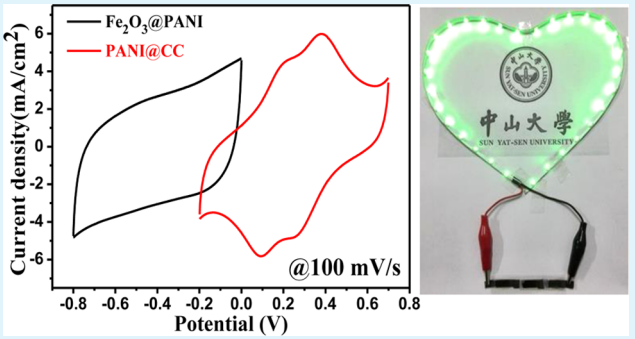

KEYWORDS: *α-Fe_2O_3@PANI, hybrid, core–shell nanowire, negative electrode, supercapacitor*

1. INTRODUCTION

Supercapacitors have mainly been employed as energy sources for back-up power devices, hybrid electronic vehicles, and renewable energy systems due to their high power density, long cycling life, safety, and low maintenance costs.[1] However, in order to meet the increasing energy density demands for next-generation electronic devices, the energy density of supercapacitor needs to be further improved. Compared with symmetric supercapacitors (SSCs), the asymmetric supercapacitors (ASCs) demonstrate better performance because of their much wider voltage windows and thus the increased energy density.[2,3] The ASC devices typically consist of a cathode as the energy source and an anode as the power source.[4,5] Due to their large surface area, excellent electrical conductivity, and outstanding stability, carbon-based materials have been widely used as anodes for ASCs.[6−8] However, the low specific capacitance (C_{sp}) of carbon materials severely limits the energy density of ASCs according to the equation of $1/C = 1/C_{an} + 1/C_{cat}$ (C_{an}, capacitance of anode; C_{cat}, capacitance of cathode).

In order to improve the energy density of ASCs, it is highly desirable to explore new anode materials with high capacitance and conductivity. In this regard, some new negative electrodes, such as MoO_{3-x},[9,10] Fe_2O_3,[11,12] and some metal nitrides[13,14] have been developed for ASCs. Among these negative electrodes, hematite (α-Fe_2O_3) holds great promise for ASCs because of its high theoretical C_{sp}, suitable potential window, low cost, abundance, and nontoxicity.[15,16] However, due to its poor electrical conductivity, its electrochemical performance is mostly inferior.[17] Tremendous efforts have been devoted to address this issue, including two main directions: nanostructures and composites. The unique nanostructures, such as nanoparticles,[18,19] nanotubes,[12,20] and nanoflakes,[21,22] provide a short transport path for ions, a highly active contact area, and an effective buffer during charge–discharge processes.[23] Another strategy is to combine these nanostructures with conductive materials including carbon-based materials[17,24] and conducting polymers.[16,25−27] However, carbon coatings, which are realized usually by thermal decomposition of carbon precursors, usually cause environmental problems because of the formation of volatile organic compounds, CO and CO_2, and sometimes lead to the inferior reconstruction of materials.[28,29] The conductive polymer coating will be a good route for the enhancement of C_{sp} and stability of α-Fe_2O_3.

Herein, we first fabricated α-Fe_2O_3 nanowire arrays on carbon cloth by electrodeposition followed by an annealing process in air. Subsequently, a thin PANI was electrodeposited on the α-Fe_2O_3 nanowires and finally the highly ordered 3D α-Fe_2O_3@PANI core–shell nanowire arrays were obtained. Compared with pure α-Fe_2O_3electrode, the α-Fe_2O_3@PANI electrode has better electrochemical performance with a twice increase in C_{sp} from 33.93 to 103 mF/cm^2. In addition, a high-

Received: April 19, 2015
Accepted: June 19, 2015
Published: June 19, 2015

DOI: 10.1021/acsami.5b03126
ACS Appl. Mater. Interfaces 2015, 7, 14843−14850

Scheme 1. Schematic Illustration of the Electrode Fabrication and a Magnified View of a Single α-Fe_2O_3@PANI Core−Shell Nanowire Structure

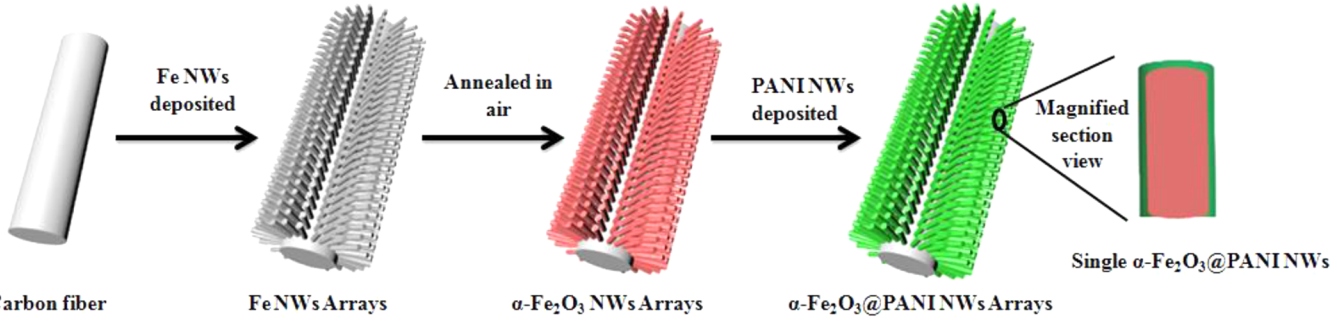

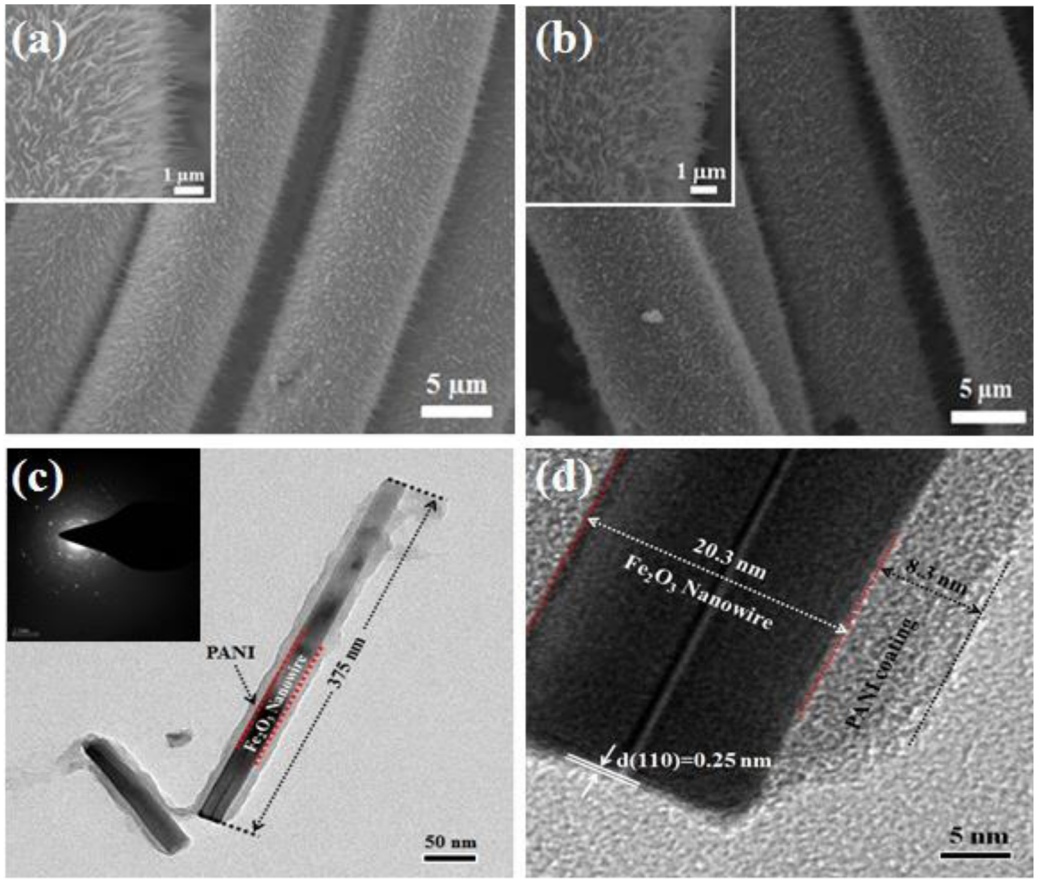

Figure 1. SEM images of (a) α-Fe_2O_3 and (b) α-Fe_2O_3@PANI; (c) TEM image, (d) HRTEM image, and (c, inset) the corresponding SAED pattern of the α-Fe_2O_3@PANI core−shell nanowire.

performance ASC was designed with α-Fe_2O_3@PANI nanowires grown on carbon as anode and PANI nanorods grown on carbon cloth as cathode, and it displayed a high volumetric capacitance of 2.02 mF/cm^3, a high energy density of 0.35 mWh/cm^3 at the power density of 120.51 mW/cm^3 based on volume of the whole device, and very good stability with C_{sp} retention of 95.77% after 10 000 cycles.

2. EXPERIMENTAL SECTION

2.1. Fabrication of Electrode Materials. All the chemical reagents used in this study were of analytical grade (AR). The electrodeposition was carried out in a simple two-electrode cell via galvanostatic electrolysis, and the graphite electrode was used as a counter electrode (spectral grade, 1.8 cm^2). Carbon cloth (0.5 × 2 cm^2) was used as the working electrode for electrodeposition, and it was washed with ethanol and water, successively, in an ultrasonic bath for 5 min.

2.1.1. Synthesis of Negative Electrode. First, metal Fe nanowire arrays were electrodeposited in a solution of 9 g/L $FeCl_3{\cdot}6H_2O$ + 14 g/L $(NH_4)_2C_2O_4{\cdot}H_2O$ at a current density of 4 mA/cm^2 at room temperature for 40 min. Then, α-Fe_2O_3 nanowire arrays were obtained by calcining Fe nanowires at 500 °C for 2 h in air with a speed of 3 °C/min. Finally, a thin PANI film was electrodeposited on the α-Fe_2O_3 nanowires in a solution 0.01 M aniline + 0.1 M H_2SO_4 with a current density of 2 mA/cm^2 at room temperature for 5 min.

2.1.2. Synthesis of Positive Electrode. PANI nanorods was electrodeposited on carbon clothin a solution 0.1 M aniline +1.0 M H_2SO_4 with a current density of 2 mA/cm^2 at room temperature for 20 min.

2.2. Fabrication of ASC. The ASC device was assembled using α-Fe_2O_3@PANI electrode (0.35 cm^2) and PANI electrode (0.35 cm^2)

DOI: 10.1021/acsami.5b03126
ACS Appl. Mater. Interfaces 2015, 7, 14843−14850

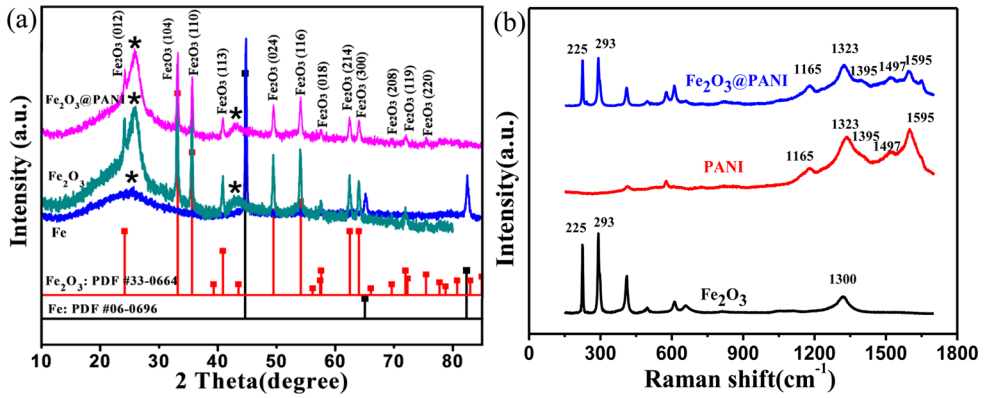

Figure 2. (a) XRD patterns of the prepared Fe, α-Fe_2O_3, and α-Fe_2O_3@PANI; (b) Raman spectrum of the prepared α-Fe_2O_3, PANI, and α-Fe_2O_3@PANI.

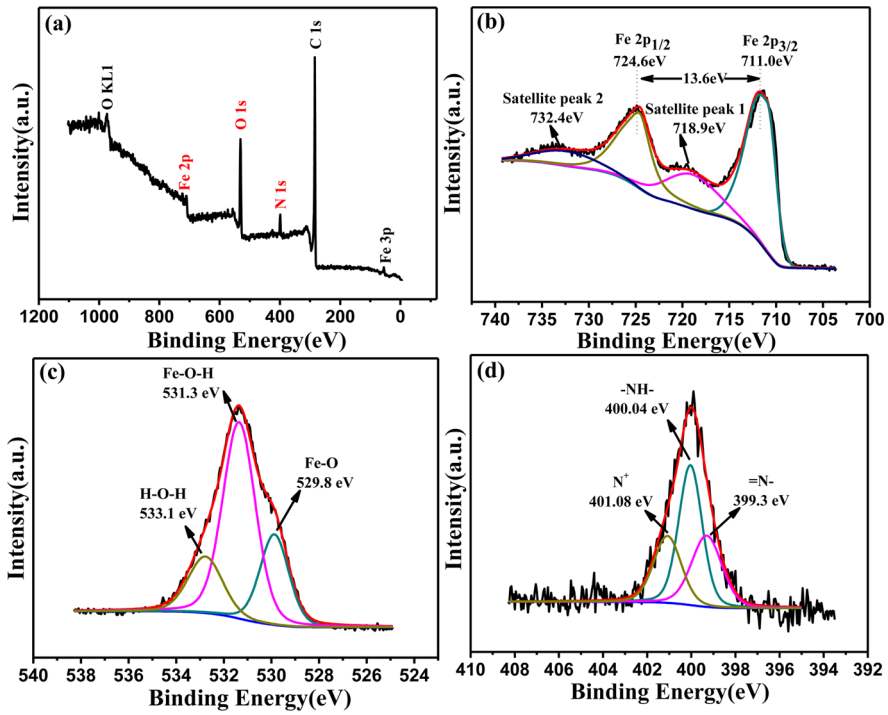

Figure 3. XPS spectra of the prepared α-Fe_2O_3@PANI: (a) survey, (b) Fe 2p, (c) O 1s, and (d) N 1s.

with a separator (NKK separator; Nippon Kodoshi Corporation, Kochi, Japan) sandwiched between the two electrodes. A Na_2SO_4 (1.0 M) aqueous solution was used as the electrolyte. To avoid leakage of the electrolyte, the entire device was sealed by two pieces of PET membranes with a small part of electrode kept outside.

2.3. Material Characterization and Electrochemical Measurements. The morphologies, microstructures, and compositions of products were characterized by field-emission scanning electron microscopy (FE-SEM, JSM-6330F), X-ray diffractometry (XRD, D-MAX 2200 VPC), transmission electron microscopy (TEM, Tecnai G2 F30), photoelectron spectroscopy (XPS, ESCA Lab250) and Raman spectroscopy (Nicolet NXR 9650).

The electrochemical measurements of the electrodes were carried out in a standard three-electrode electrolytic cell in a 1.0 M Na_2SO_4 aqueous solution. A graphite electrode was used as a counter electrode. A saturated calomel electrode (SCE) was used as the reference electrode. The cyclic voltammometry and chronopotentiometric measurements were performed on a CHI 760 E electrochemical workstation (CH Instruments, Inc.) to determine the electrochemical properties. The EIS was conducted in the frequency range between 0.01 Hz and 100 kHz with an amplitude of 5 mV at the open-circuit potential.

3. RESULTS AND DISCUSSION

The α-Fe_2O_3@PANI core−shell nanowire arrays on carbon cloth were achieved by electrodeposition, as illustrated in Scheme 1, and the electrodeposition has been proven an efficient method for synthesis of nanomaterials.[30] SEM images of α-Fe_2O_3 nanowire arrays before and after coating a thin film of PANI show that the nanowire arrays were uniformly grown on the surface of carbon fiber (Figure 1a,b). The core−shell nanostructure of α-Fe_2O_3@PANI was confirmed by TEM. As shown in Figure 1c,d, the PANI is uniformly coated on the surface of α-Fe_2O_3 nanowire. The length of the core−shell nanowire is ~375 nm. The diameter of Fe_2O_3 nanowire is ~20.3 nm, and the thickness of PANI shell is ~8.3 nm. The lattice spacing of 0.25 nm corresponds to the (110) crystal plane of α-Fe_2O_3, and a clear twin plane is seen in Figure 1d. The selected-area electron diffraction (SAED) pattern in the

DOI: 10.1021/acsami.5b03126
ACS Appl. Mater. Interfaces 2015, 7, 14843−14850

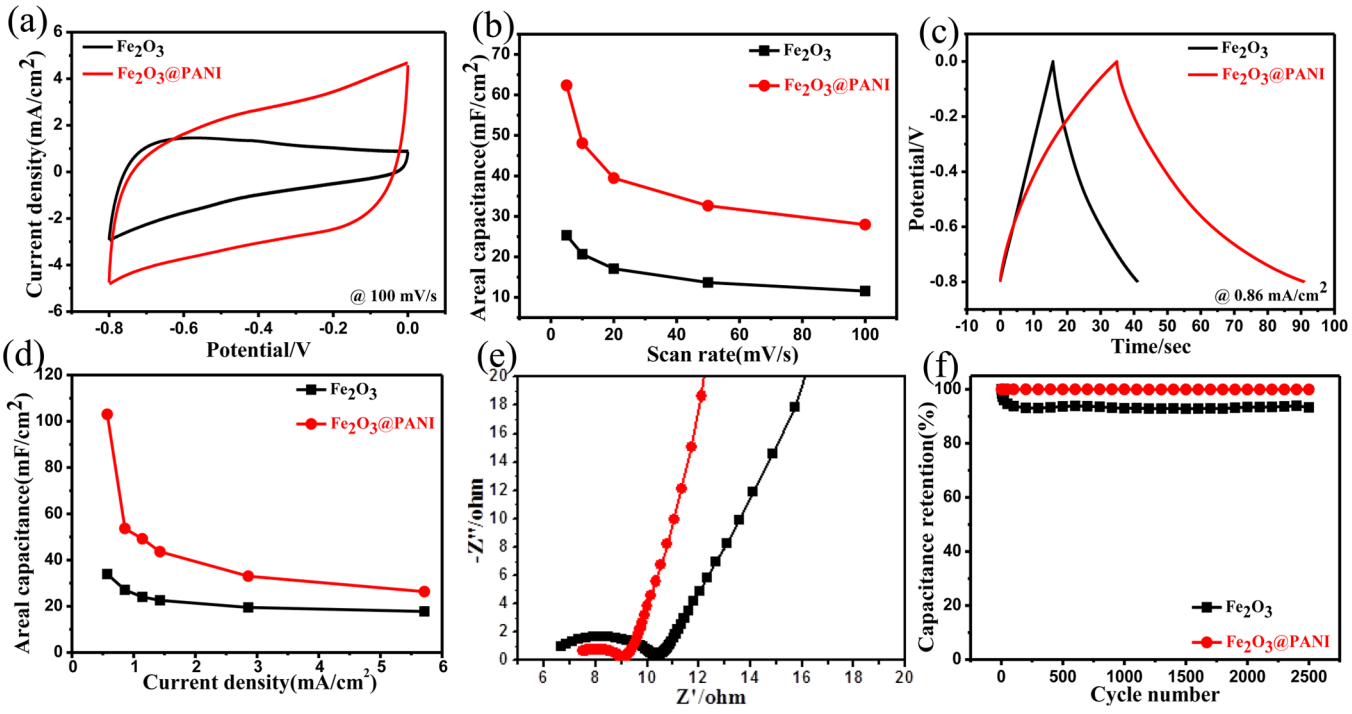

Figure 4. (a) CVs at a scan rate of 100 mV/s; (b) summary plots of areal specific capacitance versus different scan rates; (c) GCD curves at a current density of 0.86 mA/cm^2; (d) summary plot of areal specific capacitance versus different current density; (e) EIS spectrum; (f) cycle stability at 100 mV/s for 2500 cycles for α-Fe_2O_3 (black curves) and α-Fe_2O_3@PANI (red curves), which were tested in three-electrode system with 1.0 M Na_2SO_4 as the electrolyte.

inset of Figure 1c shows the polycrystalline structure of α-Fe_2O_3. The PANI layer is amorphous, and no crystal plane is seen in Figure 1d.

The α-Fe_2O_3@PANI core−shell nanowire arrays were further studied by XRD and Raman spectroscopy as shown in Figure 2, respectively. As shown in Figure 2a, we first obtained Fe nanowires on carbon cloth during the first-step electrodeposition (PDF# 06-0696), and then annealed them in air at 500 °C for 2 h with a speed of 3 °C/min to form α-Fe_2O_3.[16,31,32] The peaks of α-Fe_2O_3 are clearly seen in Figure 2a (PDF# 33-0664). After PANI coating, the peaks of α-Fe_2O_3 decrease in intensity, and this can be attributed to uniformly coating PANI on the surface of α-Fe_2O_3 nanowires. Except for the strong peaks, there are a broad peak and a weak peak (marked with star symbol) that are belong to the carbon cloth substrate (PDF# 41-1487). In Figure 2b, α-Fe_2O_3 nanowires show the characteristic Raman peaks at 225, 293, 411, and 1300 cm^{-1}.[25,33] After PANI coating, these peaks decrease in intensity and some other new peaks appear at 1165 cm^{-1} (C−H bending of benzenoid rings), 1497 cm^{-1} (C═N stretching of the quinoid rings), and 1595 cm^{-1} (C−C stretching of benzenoid rings).[34,35] In addition, two distinct peaks at 1323 and 1395 cm^{-1} can be assigned to the stretching vibrations of C−N$^+$ fragments, indicating the emeraldine salt of PANI, which is a highly electrical conductive form.[34] These results reveal that PANI is coated on the surface of α-Fe_2O_3 nanowires. Figure 3a presents XPS survey of α-Fe_2O_3@PANIA nanowire arrays, which shows four elements (Fe, O, N, and C) existing in the sample. The fine XPS spectra of Fe 2p, O 1s, and N 1s are displayed in Figure 3b−d. As shown in Figure 3b, except for two shakeup satellites at ∼718.9 and 732.4 eV, two major peaks centered at around 711.0 eV for Fe $2p_{3/2}$ and 724.6 eV for Fe $2p_{1/2}$ with a spin energy separation of 13.6 eV, which is in good agreement with the reported value for α-Fe_2O_3.[12,36] The O 1s spectrum shown in Figure 3c can be deconvoluted into three components. The bands at 529.8, 531.3 and 533.1 eV can be assigned to the oxygen bond of Fe−O, Fe−O−H, and H−O−H, respectively.[12,37] The N 1s spectrum shown in Figure 3d shows that most of the nitrogen atoms are in the form of amine (−NH−) centered at 400.04 eV in benzenoid amine or amide groups. Two small additional peaks suggest that some nitrogen atoms exist as imine (═N−) form centered at 399.3 eV and positively charged nitrogen (N$^+$) form centered at 401.08 eV.[38,39] Therefore, the PANI is coated on the surface of Fe_2O_3 nanowire arrays successfully, and this is in line with the results of XRD and Raman.

The electrochemical studies of α-Fe_2O_3 nanowire arrays and α-Fe_2O_3@PANI core−shell nanowire arrays on carbon cloth were conducted by cyclic voltammetry (CV), galvanostatic charge/discharge (GCD), and electrochemical impedance spectroscopy (EIS) in a three-electrode system in 1.0 M Na_2SO_4 electrolyte. As shown in Figure 4a, the α-Fe_2O_3@PANI core−shell nanowires electrode shows better capacitance than pure α-Fe_2O_3 nanowire electrode, and the summary plot of areal C_{sp} versus different scan rates was displayed in Figure 4b. In addition, the improvement of C_{sp} is also confirmed by the GCD curves, which were displayed in Figure 4c. The summary plot of C_{sp} versus different current density was displayed in Figure 4d, and the corresponding GCDs were displayed in Figure S1c,d, (SI). The highest C_{sp} of α-Fe_2O_3@PANI is 103 mF/cm^2, which is twice that of pure α-Fe_2O_3 (33.93 mF/cm^2). The improvement of C_{sp} is attributed to the coating of PANI, which is highly conductive and thus enhances the electrical conductivity of the overall electrode. This can be seen more clearly in EIS spectrum in Figure 4e. Compared with pure α-Fe_2O_3 electrode, the α-Fe_2O_3@PANI electrode has much

DOI: 10.1021/acsami.5b03126
ACS Appl. Mater. Interfaces 2015, 7, 14843−14850

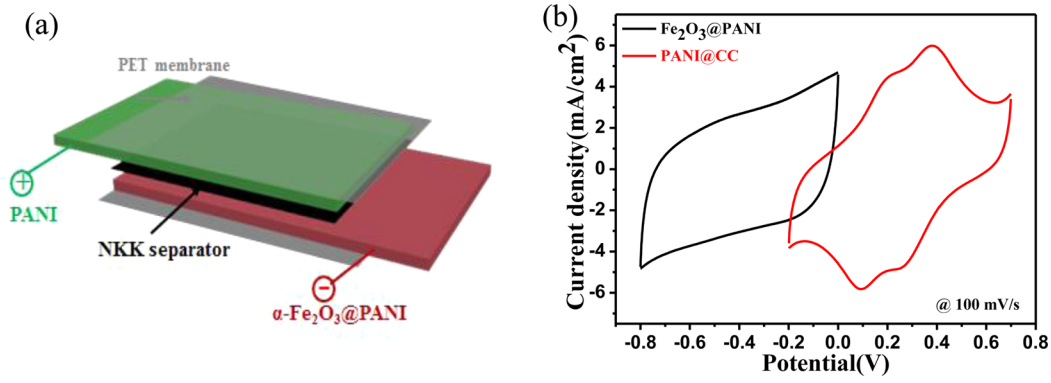

Figure 5. (a) Schematic of the structure of our flexible ASC with two electrodes separated by the TF45 (NKK) membrane (separator); (b) CVs of the α-Fe_2O_3@PANI and PANI electrodes collected at 100 mV/s in a three-electrode system.

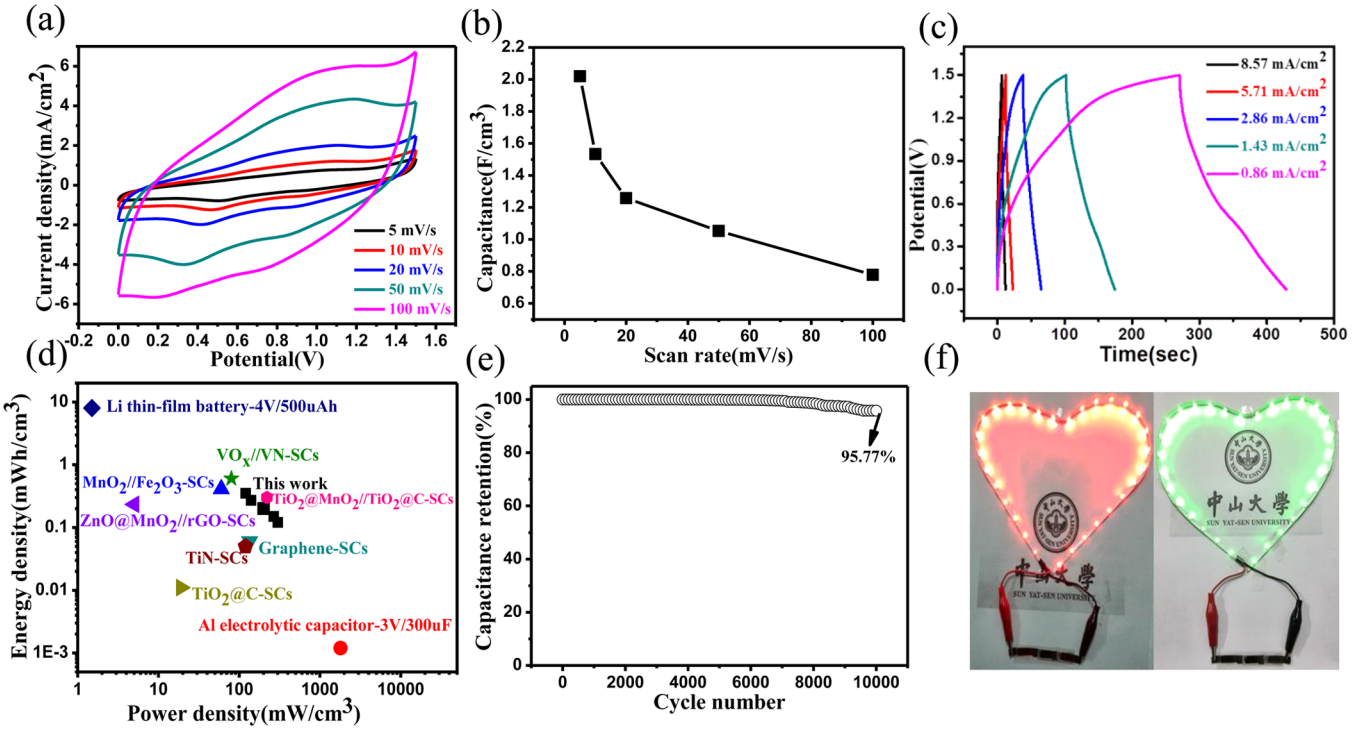

Figure 6. (a) CVs at different scan rates from 5 to 100 mV/s and (b) the summary plot of areal specific capacitance versus different scan rates. (c) GCD curves at current densities from 0.86 to 8.57 mA/cm^2. (d) Ragone plots of α-Fe_2O_3@PANI//PANI-based ASC device. The values reported for other supercapacitor (SC) devices are added for comparison. (e) Cycling stability performance of our ASC device at 50 mV/s. (f) Photographs of commercial red and green LED soft rope lights powered by our ASCs with three in series.

smaller charge-transfer resistance (R_{ct}) at high frequency, suggesting the fastest charge transfer and transport process.[40] Moreover, the low frequency line shows more vertical shape for α-Fe_2O_3@PANI electrode, indicating the faster ion diffusion behavior.[41] Besides, the coated PANI is helpful for improving the stability, which can be seen in Figure 4f. After 2500 cycles testing, the C_{sp} retention of α-Fe_2O_3@PANI is almost 100% while the retention of pure α-Fe_2O_3 is just 93%.

Therefore, such high electrochemical performance of α-Fe_2O_3@PANI electrode can be attributed to the synergistic effect of α-Fe_2O_3 and PANI. Moreover, the carbon cloth can act as conductivity framework, and the active materials were grown directly on its interconnected carbon fibers, which ensure a good electric contact and consequently enhances the rate capability.[42] In additional, the hierarchical 3D core−shell nanowire arrays structure provides large reaction surface area, fast ion and electron transfer, and good structural stability.[43] Significantly, the excellent capacitive behaviors demonstrate that the prepared α-Fe_2O_3@PANI will be a promising candidate as a negative electrode for ASCs.

To fabricate ASCs using α-Fe_2O_3@PANI core−shell nanowires as the negative electrode, we select PANI as the positive electrode because of its high capacitance (theoretical value: 3407 F/g) and easy synthesis. Moreover, PANI has high hydrogen evolution overpotential and large operational potential.[44,45] In our experiments, PANI nanorods were electrodeposited on carbon cloth by a similar method for coating PANI on α-Fe_2O_3. The morphology and its electrochemical performance in three-electrode system were displayed in Figure S2 (SI). Obviously, there is a pair of redox peaks, which are attributed to the redox transitions of PANI (i.e., the leucoemeraldine/emeraldine transitions and the emeraldine/

DOI: 10.1021/acsami.5b03126
ACS Appl. Mater. Interfaces 2015, 7, 14843−14850

pernigraniline transition).[46] Figure 5a shows the schematic illustration of the structure of our ASC, which is sealed by two thin pieces of PET membranes. To determine the best operating potential of the ASC device, the CVs of α-Fe_2O_3@PANI electrode (black curve) and PANI (red curve) electrode were measured in a 1.0 M Na_2SO_4 solution, respectively, as shown in Figure 5b. Figure S3 (SI) displays the CV curves and GCD curves of the prepared ASC device collected in different potential windows, which indicates that the potential window of the fabricated ASC can be as large as 1.5 V (vs SCE).

Figure 6a shows the CV of the ASC at different scan rates from 5 to 100 mV/s. The current intensity increases as the scan rate increases, but the shape is well retained, indicating its ideal pseudocapacitive nature. Figure 6b shows the volume capacitance as a function of scan rate, and the volume capacitance increases from 0.78 to 2.02 F/cm^3 with the scan rate from 100 to 5 mV/s. Figure 6c shows the GCD test, which was performed at different current densities in the potential window of 0−1.5 V (vs SCE). The linear voltage versus time profiles, the symmetrical charge/discharge characteristics, and a quick $I-V$ response represents good capacitive characteristics for the ASC. Figure 6d compares the volumetric power density and energy density of the ASC device to the values reported for other supercapacitors. The maximum energy density of the prepared ASC is 0.35 mWh/cm^3 at a power density of 120.51 mW/cm^3. These values are superior to the previously reported supercapacitor systems, including graphene-based SCs (0.06 mWh/cm^3, 135 mW/cm^3),[47] TiN-based SCs (0.05 mWh/cm^3, 120 mW/cm^3),[48] TiO_2@C-based SCs (0.01 mWh/cm^3, 19 mW/cm^3),[49] ZnO@MnO_2//rGO-based SCs (0.234 mWh/cm^3, 5 mW/cm^3),[50] and even comparable to the values of MnO_2//Fe_2O_3-based SCs (0.4 mWh/cm^3, 60 mW/cm^3),[11] VO_x//VN-based SCs (0.6 mWh/cm^3, 80 mW/cm^3),[13] and TiO_2@MnO_2//TiO_2@ C-based SCs (0.3 mWh/cm^3, 190 mW/cm^3).[3] In addition, the ASC exhibits good cycling stability, which is one of the most critical factors in supercapacitor operations. The cycling test of the ASC shows ~95.77% C_{sp} retention over 10 000 cycles at a scan rate of 50 mV/s (Figure 6e), which is significantly better than those reported in previous work (typically 70−85% retention over 1000 cycles).[51,52] To show the practical application, we assembled three ASCs in series. As shown in Figure 6f, the ASCs can light a 50 cm long commercial red (2.0 V) or green (2.5 V) LED soft rope light, indicating high power and energy characteristic of the ASCs device.

4. CONCLUSIONS

In summary, we fabricated highly ordered α-Fe_2O_3@PANI core−shell nanowire arrays by a simple and cost-effective electrodeposition method and first used them as negative electrodes for supercapacitors. This unique core−shell nanowire array structure enables a high areal C_{sp} of 103 mF/cm^2 and outstanding cycling performance (2500 cycles without any loss), which are superior to pure α-Fe_2O_3 nanowire arrays. Additionally, a high-performance ASC device based on α-Fe_2O_3@PANI core−shell nanowire arrays as anode and PANI nanowire arrays as cathode was prepared. The α-Fe_2O_3@PANI// PANI ASC device achieved a maximum energy density of 0.35 mWh/cm^3 and a maximum power density of 301.19 mW/cm^3 with a good cycling stability of 95.77% C_{sp} retention after 10 000 cycles. These findings will open up the possibility of α-Fe_2O_3@PANI core−shell nanowire arrays as anodes for the applications in ASCs with large potential window and high energy and power densities to meet the diverse demands in the modern industry development.

■ ASSOCIATED CONTENT

Supporting Information

Calculations of specific capacitance, power density, and energy density; CVs, galvanostatic data, and SEM image. The Supporting Information is available free of charge on the ACS Publications website at DOI: 10.1021/acsami.5b03126.

■ AUTHOR INFORMATION

Corresponding Author

* E-mail: ligaoren@mail.sysu.edu.cn. Fax: 86-20-84112245. Tel: 86-20-84110071.

Notes

The authors declare no competing financial interest.

■ ACKNOWLEDGMENTS

This work was supported by NSFC (51173212 and J1103305), Natural Science Foundation of Guangdong Province (S2013020012833), Fundamental Research Fund for the Central Universities (13lgpy51), SRF for ROCS, SEM ([2012]1707), the Project of High Level Talents in Higher School of Guangdong Province, and Open-End Fund of Key Laboratory of Functional Inorganic Material Chemistry (Heilongjiang University), Ministry of Education.

■ REFERENCES

(1) Simon, P.; Gogotsi, Y. Materials for Electrochemical Capacitors. *Nat. Mater.* **2008**, *7*, 845−854.

(2) Yan, J.; Fan, Z. J.; Sun, W.; Ning, G. Q.; Wei, T.; Zhang, Q.; Zhang, R. F.; Zhi, L. J.; Wei, F. Advanced Asymmetric Supercapacitors Based on Ni(OH)$_2$/Graphene and Porous Graphene Electrodes with High Energy Density. *Adv. Funct. Mater.* **2012**, *22*, 2632−2641.

(3) Lu, X.; Yu, M.; Wang, G.; Zhai, T.; Xie, S.; Ling, Y.; Tong, Y.; Li, Y. H-TiO_2@MnO_2//H-TiO_2@C Core-Shell Nanowires for High Performance and Flexible Asymmetric Supercapacitors. *Adv. Mater.* **2013**, *25*, 267−272.

(4) Lu, X.; Yu, M.; Wang, G.; Tong, Y.; Li, Y. Flexible Solid-State Supercapacitors: Design, Fabrication and Applications. *Energy Environ. Sci.* **2014**, *7*, 2160−2181.

(5) Feng, J.-X.; Ye, S.-H.; Wang, A.-L.; Lu, X.-F.; Tong, Y.-X.; Li, G.-R. Flexible Cellulose Paper-Based Asymmetrical Thin Film Supercapacitors with High-Performance for Electrochemical Energy Storage. *Adv. Funct. Mater.* **2014**, *24*, 7093−7101.

(6) Liu, L.; Niu, Z.; Zhang, L.; Zhou, W.; Chen, X.; Xie, S. Nanostructured Graphene Composite Papers for High Flexible and Foldable Supercapacitors. *Adv. Mater.* **2014**, *26*, 4855−4862.

(7) Dai, L.; Chang, D. W.; Baek, J. B.; Lu, W. Carbon Nanomaterials for Advanced Energy Conversion and Storage. *Small* **2012**, *8*, 1130−1166.

(8) Tang, C. H.; Yin, X.; Gong, H. Superior Performance Asymmetric Supercapacitors Based on a Directly Grown Commercial Mass 3D Co_3O_4@Ni(OH)$_2$ Core-Shell Electrode. *ACS Appl. Mater. Interfaces* **2013**, *5*, 10574−10582.

(9) Chang, J.; Jin, M.; Yao, F.; Kim, T. H.; Le, V. T.; Yue, H.; Gunes, F.; Li, B.; Ghosh, A.; Xie, S.; Lee, Y. H. Asymmetric Supercapacitors Based on Graphene/MnO_2 Nanospheres and Graphene/MoO_3 Nanosheets with High Energy Density. *Adv. Funct. Mater.* **2013**, *23*, 5074−5083.

(10) Li, G. R.; Wang, Z. L.; Zheng, F. L.; Ou, Y.; Tong, Y. X. ZnO@MoO_3 Core/Shell Nanocables: Facile Electrochemical Synthesis and Enhanced Supercapacitor Performances. *J. Mater. Chem.* **2011**, *21*, 4217−4221.

(11) Lu, X.; Zeng, Y.; Yu, M.; Zhai, T.; Liang, C.; Xie, S.; Balogun, M. S.; Tong, Y. Oxygen-Deficient Hematite Nanorods as High-Perform-

DOI: 10.1021/acsami.5b03126
ACS Appl. Mater. Interfaces 2015, 7, 14843−14850

ance and Novel Negative Electrodes for Flexible Asymmetric Supercapacitors. *Adv. Mater.* **2014**, *26*, 3148−3155.
(12) Yang, P.; Ding, Y.; Lin, Z.; Chen, Z.; Li, Y.; Qiang, P.; Ebrahimi, M.; Mai, W.; Wong, C. P.; Wang, Z. L. Low-Cost High-Performance Solid-State Asymmetric Supercapacitors Based on MnO_2 Nanowires and Fe_2O_3 Nanotubes. *Nano Lett.* **2014**, *14*, 731−736.
(13) Lu, X.; Yu, M.; Zhai, T.; Wang, G.; Xie, S.; Liu, T.; Liang, C.; Tong, Y.; Li, Y. High Energy Density Asymmetric Quasi-solid-state Supercapacitor Based on Porous Vanadium Nitride Nanowire Anode. *Nano Lett.* **2013**, *13*, 2628−2633.
(14) Lee, K.-H.; Lee, Y.-W.; Ko, A. R.; Cao, G.; Park, K.-W.; Vyas, B. Single-Crystalline Mesoporous Molybdenum Nitride Nanowires with Improved Electrochemical Properties. *J. Am. Ceram. Soc.* **2013**, *96*, 37−39.
(15) Tian, W.; Wang, X.; Zhi, C.; Zhai, T.; Liu, D.; Zhang, C.; Golberg, D.; Bando, Y. $Ni(OH)_2$ Nanosheet@Fe_2O_3 Nanowire Hybrid Composite Arrays for High-Performance Supercapacitor Electrodes. *Nano Energy* **2013**, *2*, 754−763.
(16) Jeong, J. M.; Choi, B. G.; Lee, S. C.; Lee, K. G.; Chang, S. J.; Han, Y. K.; Lee, Y. B.; Lee, H. U.; Kwon, S.; Lee, G.; Lee, C. S.; Huh, Y. S. Hierarchical Hollow Spheres of Fe_2O_3@Polyaniline for Lithium Ion Battery Anodes. *Adv. Mater.* **2013**, *25*, 6250−6255.
(17) Lee, K.; Deng, S.; Fan, H. M.; Mhaisalkar, S.; Tan, H.; Tok, E. S.; Loh, K.; Chin, W.; Sow, C. H. α-Fe_2O_3 Nanotubes-reduced Graphene Oxide Composites as Synergistic Electrochemical Capacitor Materials. *Nanoscale* **2012**, *4*, 2958−2961.
(18) Son, M. Y.; Hong, Y. J.; Lee, J.-K.; Chan Kang, Y. One-pot Synthesis of Fe_2O_3 Yolk-shell Particles with two, three, and four Shells for Application as an Anode Material in Lithium-ion Batteries. *Nanoscale* **2013**, *5*, 11592−11597.
(19) Ma, J. M.; Lian, J. B.; Duan, X. C.; Liu, X. D.; Zheng, W. J. α-Fe_2O_3: Hydrothermal Synthesis, Magnetic and Electrochemical Properties. *J. Phys. Chem. C* **2010**, *114*, 10671−10676.
(20) Xie, K.; Li, J.; Lai, Y.; Lu, W.; Zhang, Z. a.; Liu, Y.; Zhou, L.; Huang, H. Highly Ordered Iron Oxide Nanotube Arrays as Electrodes for Electrochemical Energy Storage. *Electrochem. Commun.* **2011**, *13*, 657−660.
(21) Reddy, M. V.; Yu, T.; Sow, C. H.; Shen, Z. X.; Lim, C. T.; Subba Rao, G. V.; Chowdari, B. V. R. α-Fe_2O_3 Nanoflakes as an Anode Material for Li-Ion Batteries. *Adv. Funct. Mater.* **2007**, *17*, 2792−2799.
(22) Zhu, J.; Huang, L.; Xiao, Y.; Shen, L.; Chen, Q.; Shi, W. Hydrogenated CoO_x Nanowire@$Ni(OH)_2$ Nanosheet Core-shell Nanostructures for High-Performance Asymmetric Supercapacitors. *Nanoscale* **2014**, *6*, 6772−6781.
(23) Luo, J.; Liu, J.; Zeng, Z.; Ng, C. F.; Ma, L.; Zhang, H.; Lin, J.; Shen, Z.; Fan, H. J. Three-Dimensional Graphene Foam Supported Fe_3O_4 Lithium Battery Anodes with Long Cycle Life and High Rate Capability. *Nano Lett.* **2013**, *13*, 6136−6143.
(24) Lee, S. H.; Sridhar, V.; Jung, J. H.; Karthikeyan, K.; Lee, Y. S.; Mukherjee, R.; Koratkar, N.; Oh, I. K. Graphene-Nanotube-Iron Hierarchical Nanostructure as Lithium Ion Battery Anode. *ACS Nano* **2013**, *7*, 4242−4251.
(25) Liu, J.; Zhou, W.; Lai, L.; Yang, H.; Hua Lim, S.; Zhen, Y.; Yu, T.; Shen, Z.; Lin, J. Three Dimensionals α-Fe_2O_3/Polypyrrole (Ppy) Nanoarray as Anode for Micro Lithium Ion Batteries. *Nano Energy* **2013**, *2*, 726−732.
(26) Zhou, C.; Zhang, Y.; Li, Y.; Liu, J. Construction of High-Capacitance 3D CoO@Polypyrrole Nanowire Array Electrode for Aqueous Asymmetric Supercapacitor. *Nano Lett.* **2013**, *13*, 2078−2085.
(27) Xia, X.; Chao, D.; Fan, Z.; Guan, C.; Cao, X.; Zhang, H.; Fan, H. J. A New Type of Porous Graphite Foams and Their Integrated Composites with Oxide/Polymer Core/Shell Nanowires for Supercapacitors: Structural Design, Fabrication, and Full Supercapacitor Demonstrations. *Nano Lett.* **2014**, *14*, 1651−1658.
(28) Lepage, D.; Michot, C.; Liang, G.; Gauthier, M.; Schougaard, S. B. A Soft Chemistry Approach to Coating of $LiFePO_4$ with a Conducting Polymer. *Angew. Chem., Int. Ed.* **2011**, *50*, 6884−6887.
(29) Wang, F.; Zhan, X.; Cheng, Z.; Wang, Z.; Wang, Q.; Xu, K.; Safdar, M.; He, J. Tungsten Oxide@Polypyrrole Core-Shell Nanowire Arrays as Novel Negative Electrodes for Asymmetric Supercapacitors. *Small* **2015**, *11*, 749−755.
(30) Hodes, G. *Electrochemistry of Nanomaterials*; Wiley-VCH: Weinheim, Germany, 2008.
(31) Wang, B.; Chen, J. S.; Wu, H. B.; Wang, Z.; Lou, X. W. Quasiemulsion-Templated Formation of α-Fe_2O_3 Hollow Spheres with Enhanced Lithium Storage Properties. *J. Am. Chem. Soc.* **2011**, *133*, 17146−17148.
(32) Liu, S.; Chen, Z.; Xie, K.; Li, Y.; Xu, J.; Zheng, C. A Facile One-step Hydrothermal Synthesis of α-Fe_2O_3 Nanoplates Imbedded in Graphene Networks with High-rate Lithium Storage and Long Cycle Life. *J. Mater. Chem. A* **2014**, *2*, 13942−13948.
(33) Mao, Y.; Kong, Q.; Guo, B.; Fang, X.; Guo, X.; Shen, L.; Armand, M.; Wang, Z.; Chen, L. Polypyrrole-iron-oxygen Coordination Complex as High Performance Lithium Storage Material. *Energy Environ. Sci.* **2011**, *4*, 3442−3447.
(34) Drury, A.; Chaure, S.; Kröll, M.; Nicolosi, V.; Chaure, N.; Blau, W. J. Fabrication and Characterization of Silver/Polyaniline Composite Nanowires in Porous Anodic Alumina. *Chem. Mater.* **2007**, *19*, 4252−4258.
(35) Yao, Q.; Chen, L.; Zhang, W.; Liufu, S.; Chen, X. Enhanced Thermoelectric Performance of Single-Walled Carbon Nanotubes/Polyaniline Hybrid Nanocomposites. *ACS Nano* **2010**, *4*, 2445−2451.
(36) Yamashita, T.; Hayes, P. Analysis of XPS Spectra of Fe^{2+} and Fe^{3+} Ions in Oxide Materials. *Appl. Surf. Sci.* **2008**, *254*, 2441−2449.
(37) Long, C. L.; Jiang, L. L.; Wei, T.; Yan, J.; Fan, Z. J. High-Performance Asymmetric Supercapacitors with Lithium Intercalation Reaction Using Metal Oxide-Based Composites as Electrode Materials. *J. Mater. Chem. A* **2014**, *2*, 16678−16686.
(38) Zhang, K.; Zhang, L.; Zhao, X. S.; Wu, J. Graphene/Polyaniline Nanofiber Composites as Supercapacitor Electrodes. *Chem. Mater.* **2010**, *22*, 1392−1401.
(39) Park, H. W.; Kim, T.; Huh, J.; Kang, M.; Lee, J. E.; Yoon, H. Anisotropic Growth Control of Polyaniline Nanostructures and Their Morphology-Dependent Electrochemical Characteristics. *ACS Nano* **2012**, *6*, 7624−7633.
(40) Justin, P.; Meher, S. K.; Rao, G. R. Tuning of Capacitance Behavior of NiO Using Anionic, Cationic, and Nonionic Surfactants by Hydrothermal Synthesis. *J. Phys. Chem. C* **2010**, *114*, 5203−5210.
(41) Li, L.; Cheah, Y.; Ko, Y.; Teh, P.; Wee, G.; Wong, C.; Peng, S.; Srinivasan, M. The Facile Synthesis of Hierarchical Porous Flower-like $NiCo_2O_4$ with Superior Lithium Storage Properties. *J. Mater. Chem. A* **2013**, *1*, 10935−10941.
(42) Lu, X. F.; Wu, D. J.; Li, R. Z.; Li, Q.; Ye, S. H.; Tong, Y. X.; Li, G. R. Hierarchical $NiCo_2O_4$ Nanosheets@Hollow Microrod Arrays for High-performance Asymmetric Supercapacitors. *J. Mater. Chem. A* **2014**, *2*, 4706−4713.
(43) Mai, L.; Tian, X.; Xu, X.; Chang, L.; Xu, L. Nanowire Electrodes for Electrochemical Energy Storage Devices. *Chem. Rev.* **2014**, *114*, 11828−11862.
(44) Bai, M.-H.; Liu, T.-Y.; Luan, F.; Li, Y.; Liu, X.-X. Electrodeposition of Vanadium Oxide-polyaniline Composite Nanowire Electrodes for High Energy Density Supercapacitors. *J. Mater. Chem. A* **2014**, *2*, 10882−10888.
(45) Wang, K.; Wu, H.; Meng, Y.; Wei, Z. Conducting Polymer Nanowire Arrays for High Performance Supercapacitors. *Small* **2014**, *10*, 14−31.
(46) Xu, J.; Wang, K.; Zu, S.-Z.; Han, B.-H.; Wei, Z. Hierarchical Nanocomposites of Polyaniline Nanowire Arrays on Graphene Oxide Sheets with Synergistic Effect for Energy Storage. *ACS Nano* **2010**, *4*, 5019−5026.
(47) Xu, Y.; Lin, Z.; Huang, X.; Liu, Y.; Huang, Y.; Duan, X. Flexible Solid-State Supercapacitors Based on Three-Dimensional Graphene Hydrogel Films. *ACS Nano* **2013**, *7*, 4042−4049.
(48) Lu, X.; Wang, G.; Zhai, T.; Yu, M.; Xie, S.; Ling, Y.; Liang, C.; Tong, Y.; Li, Y. Stabilized TiN Nanowire Arrays for High-performance and Flexible Supercapacitors. *Nano Lett.* **2012**, *12*, 5376−5381.

DOI: 10.1021/acsami.5b03126
ACS Appl. Mater. Interfaces 2015, 7, 14843−14850

(49) Zheng, H.; Zhai, T.; Yu, M.; Xie, S.; Liang, C.; Zhao, W.; Wang, S. C. I.; Zhang, Z.; Lu, X. TiO_2@C Core−Shell Nanowires for High-performance and Flexible Solid-state Supercapacitors. *J. Mater. Chem. C* **2013**, *1*, 225−229.
(50) Zilong, W.; Zhu, Z.; Qiu, J.; Yang, S. High Performance Flexible Solid-state Asymmetric Supercapacitors from MnO_2/ZnO Core-shell Nanorods//Specially Reduced Graphene Oxide. *J. Mater. Chem. C* **2014**, *2*, 1331−1336.
(51) Wu, Z. S.; Ren, W.; Wang, D.; Li, F.; Liu, B.; Cheng, H. M. High-energy MnO_2 Nanowire/Graphene and Graphene Asymmetric Electrochemical Capacitors. *ACS Nano* **2010**, *4*, 5835−5842.
(52) Chen, S.; Zhu, J.; Wu, X.; Han, Q.; Wang, X. Graphene Oxide MnO_2 Nanocomposites for Supercapacitors. *ACS Nano* **2010**, *4*, 2822−2830.

DOI: 10.1021/acsami.5b03126
ACS Appl. Mater. Interfaces 2015, 7, 14843−14850